Determination of the Absolute Configurations of Natural Products via Density Functional Theory Calculations of Optical Rotation, Electronic Circular Dichroism, and Vibrational Circular Dichroism: The Cytotoxic Sesquiterpene Natural Products Quadrone, Suberosenone, Suberosanone, and Suberosenol A Acetate

P. J. Stephens,*,† D. M. McCann,† F. J. Devlin,† and A. B. Smith, III‡

Department of Chemistry, University of Southern California, Los Angeles, California 90089-0482, and Department of Chemistry, University of Pennsylvania, Philadelphia, Pennsylvania 19104-6323

Received March 14, 2006

The determination of the absolute configurations (ACs) of chiral molecules using the chiroptical techniques of optical rotation (OR), electronic circular dichroism (ECD), and vibrational circular dichroism (VCD) has been revolutionized by the development of density functional theory (DFT) methods for the prediction of these properties. Here, we demonstrate the significance of these advances for the stereochemical characterization of natural products. Time-dependent DFT (TDDFT) calculations of the specific rotations, $[\alpha]_D$, of four cytotoxic natural products, quadrone (**1**), suberosenone (**2**), suberosanone (**3**), and suberosenol A acetate (**4**), are used to assign their ACs. TDDFT calculations of the ECD of **1** are used to assign its AC. The VCD spectrum of **1** is reported and also used, together with DFT calculations, to assign its AC. The ACs of **1** derived from its $[\alpha]_D$, ECD, and VCD are identical and in agreement with the AC previously determined via total synthesis. The previously undetermined ACs of **2**−**4**, derived from their $[\alpha]_D$ values, have absolute configurations of their tricyclic cores identical to that of **1**. Further studies of the ACs of these molecules using ECD and, especially, VCD are recommended to establish more definitively this finding. Our studies of the OR, ECD, and VCD of quadrone are the first to utilize DFT calculations of all three properties for the determination of the AC of a chiral natural product molecule.

The sesquiterpene quadrone, **1**, was isolated from the fungus *Aspergillus terreus* and structurally characterized by X-ray crystallography in 1978.[1,2] The reported cytotoxicity and unusual structure

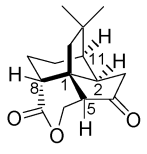

(1*R*,2*R*,5*S*,8*R*,11*R*)-**1**
Quadrone

inspired considerable synthetic activity, culminating in the total synthesis of both enantiomers of quadrone by Smith et al.,[3] which established the AC of the natural product as 1*R*,2*R*,5*S*,8*R*,11*R*-(−).

In 1996, a structurally related sesquiterpene, suberosenone, **2**, was isolated from the marine gorgonian *Subergorgia suberosa* and shown to possess potent cytotoxicity, relative to quadrone.[4] A total

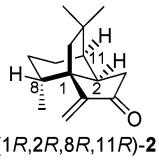

(1*R*,2*R*,8*R*,11*R*)-**2**
Suberosenone

synthesis of racemic **2** has been reported,[5] but the AC of **2** has not been determined.

In 2000, several new members of the suberosenone family were isolated from the gorgonian *Isis hippuris*, and their cytotoxicity studied.[6] Two of these were suberosanone, **3**, and suberosenol A acetate, **4**. Again, ACs were not determined.

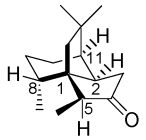

(1*R*,2*R*,5*S*,8*R*,11*R*)-**3**
Suberosanone

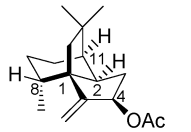

(1*R*,2*R*,4*R*,8*R*,11*R*)-**4**
Suberosenol A Acetate

Although the ACs of **2**, **3**, and **4** have not been determined, their specific rotations, $[\alpha]_D$, have been reported, as detailed in Table 1. In collaboration with J. R. Cheeseman and M. J. Frisch at Gaussian Inc., we have recently developed a new methodology for calculating the transparent spectral region specific rotations of chiral molecules using ab initio time-dependent density functional theory (TDDFT)[7] and have applied this method to the determination of the ACs of a number of organic molecules.[8] Herein, we employ TDDFT calculations of the $[\alpha]_D$ values of the sesquiterpenes **1**−**4** to determine their ACs. In the case of **1** the AC of Smith et al.[3] is confirmed. For **2**−**4**, the ACs are determined for the first time.

We have also applied the TDDFT methodology to the calculation of the ECD of chiral molecules and employed it to determine the ACs of a number of organic molecules.[8c,d] The ECD spectrum of **1** has been reported, but as yet ECD spectra for **2**−**4** have not been reported. We also report TDDFT calculations of the ECD of **1**−**4**. In the case of **1**, comparison to the experimental ECD further confirms the previously determined AC. For **2**−**4**, the calculations permit the potential utility of ECD to confirm the ACs obtained from their $[\alpha]_D$ values to be evaluated.

Prior to the development of the TDDFT methodologies for the calculation of transparent spectral region specific rotations and ECD, DFT was applied to the calculation of VCD,[10] using the Stephens equation for VCD intensities.[11] Subsequently, we have determined the ACs of a wide variety of molecules using DFT calculations of VCD spectra.[12] Here, we report the first measurements of the VCD

* To whom correspondence should be addressed. E-mail: pstephen@usc.edu. Tel: 213-740-4119.
† University of Southern California.
‡ University of Pennsylvania.

10.1021/np060112p CCC: $33.50
Published on Web 06/13/2006

Table 1. Experimental and Calculated Specific Rotations of Cytotoxins **1**−**4**

molecule	λ (nm)	$[\alpha]_\lambda$(expt)[a]	AC	$[\alpha]_\lambda$(calc)[a,b]	Δ[c]	AC	Δ[c]
1	D	−52.7[d]	1*R*,2*R*,5*S*,8*R*,11*R*	−38.8	+13.9	1*S*,2*S*,5*R*,8*S*,11*S*	+91.5
	D	−60.53[e]		−38.8	+21.73		+99.33
	D	−44.6[f]		−38.8	+5.8		+83.4
	578	−45.4[f]		−39.7	+5.7		+85.1
	546	−48.8[f]		−42.1	+6.7		+90.9
	436	−42.9[f]		−30.6	+12.3		+73.5
	365	102.6[f]		127.6	+25.0		−230.2
2	D	55.7[g]	1*R*,2*R*,8*R*,11*R*	10.5	−45.2	1*S*,2*S*,8*S*,11*S*	−66.2
	578			14.9			
	546			32.6			
	436			348.6			
	365			*i*			
3	D	−60[h]	1*R*,2*R*,5*S*,8*R*,11*R*	−20.6	+39.4	1*S*,2*S*,5*R*,8*S*,11*S*	+80.6
	578			−20.1			
	546			−17.6			
	436			35.0			
	365			300.9			
4	D	−110[h]	1*R*,2*R*,4*R*,8*R*,11*R*	−220.8	−110.8	1*S*,2*S*,4*S*,8*S*,11*S*	+330.8
	578			−230.4			
	546			−261.6			
	436			−440.3			
	365			−687.7			

[a] $[\alpha]_D$ in deg·[dm·g/cm^3]$^{-1}$. [b] B3LYP/aug-cc-pVDZ//B3LYP/6-31G*. [c] $\Delta = [\alpha]_D$(calc.) − $[\alpha]_D$(expt.). [d] Reference 3 (*c* 0.59, EtOH). [e] Reference 9 (*c* 0.5, $CHCl_3$). [f] This work, on synthetic (−)-**1** (*c* 0.12, $CDCl_3$). [g] Reference 4 (c 0.78, $CHCl_3$). [h] Reference 6 (c 0.1, $CHCl_3$). [i] Not calculated since this wavelength is resonant with the lowest electronic excitation of **2** (Figure 5).

of **1** and DFT calculations, which further confirm the previously determined AC. These results serve to demonstrate the power of the VCD/DFT methodology in determining ACs and the greater reliability of the ACs obtained than those obtained using TDDFT calculations of specific rotations and ECD, leading to the conclusion that the most reliable ACs of **2**−**4** will be provided by VCD spectroscopy.

Experimental and Computational Procedures

Conformational analysis of **1**−**4** has been carried out using a protocol described in previous publications.[8c−e,12l,m] First, a Monte Carlo search of the potential energy surface (PES) is carried out using the MMFF94 molecular mechanics force field via the SPARTAN 02 program.[13] All stable conformations obtained are then reoptimized using DFT at the B3LYP/6-31G* level. Next, the harmonic vibrational frequencies of each conformation are calculated using B3LYP/6-31G* to confirm that the conformation is stable. Last, the free energies of all conformations are calculated and equilibrium room-temperature populations obtained thence. All DFT calculations are carried out using the GAUSSIAN 03 program.[14]

Specific rotations of **1**−**4** have been calculated using TDDFT, B3LYP/6-31G* equilibrium geometries, the functional B3LYP, and the basis set aug-cc-pVDZ via GAUSSIAN 03, as detailed in previous publications.[7,8] Gauge-invariant atomic orbitals [GIAOs] are used, guaranteeing origin-independent rotations.[7b]

Electronic excitation energies, oscillator strengths, and rotational strengths of **1**−**4** have been calculated using TDDFT, B3LYP/6-31G* equilibrium geometries, the functional B3LYP, and the basis set aug-cc-pVDZ via GAUSSIAN 03, as detailed in previous publications.[8c,d] Rotational strengths are calculated in both length and velocity representations. GIAOs are not used; as a result, length and velocity rotational strengths are origin-dependent and origin-independent, respectively. Since length and velocity rotational strengths are identical in the complete basis set limit, the convergence of these values allows basis set errors to be gauged.

IR and VCD spectra of **1** have been calculated using DFT via GAUSSIAN 03, as detailed in previous publications.[10,12] The functionals B3LYP and B3PW91 and the basis set TZ2P were used. GIAOs are used in calculating atomic axial tensors (AATs); as a result, the vibrational rotational strengths obtained thence are origin-independent. IR and VCD spectra were obtained from calculated vibrational frequencies, dipole strengths, and rotational strengths using Lorentzian band shapes.[10f,g] Experimental IR and VCD spectra of a $CDCl_3$ solution of (−)-**1** were obtained using Thermo-Nicolet Nexus 670 IR and Bomem/Biotools Chiral IR spectrometers, respectively. The latter incorporates a second photoelastic modulator after the sample, permitting polarization scrambling and artifact reduction.[15] Baselines were the spectra of the $CDCl_3$ solvent.

Results and Discussion

Prior to the calculation of their specific rotations, ECD, and VCD, conformational analyses of molecules **1**−**4** must be carried out in order to define their stable conformations and the relative energies and free energies of these conformations. From the relative free energies the percentage population of each conformation in a room-temperature equilibrium mixture can be predicted. As shown below, for all four molecules **1**−**4** only one conformation is significantly populated at room temperature and, thus, all of these molecules are effectively conformationally rigid. For each molecule, $[\alpha]_D$, the ECD spectrum, and the VCD spectrum are then predicted for this conformation. Comparison to experimental data, where available, then allows ACs to be determined.

Conformational Analysis. Initial conformational analyses of **1**−**4** have been carried out using Monte Carlo searching together with the MMFF94 molecular mechanics force field. All stable conformations obtained are then optimized using DFT at the B3LYP/6-31G* level and the harmonic vibrational frequencies of each conformation calculated using B3LYP/6-31G* to confirm their stability. Last, the free energies of all conformations are calculated.

In the case of **1**, three stable conformations, **a**−**c**, are identified. Calculated relative energies and free energies are given in Table 2. The MMFF94 and B3LYP/6-31G* relative energies are very similar. The B3LYP/6-31G* relative energies and free energies are also very similar. Using the B3LYP/6-31G* relative free energies, equilibrium populations at room temperature can be calculated and are also given in Table 2. The population of the most stable conformation, **a**, is predicted to be >99%; effectively, **1** is a conformationally rigid molecule. Key dihedral angles of the B3LYP/6-31G* structure of conformation **a** of **1** are listed in Table 3. The cyclohexane ring C1C2C11C10C9C8 has a chair conformation, while the lactone ring C1C5C6 O C7C8 has a boat conformation. The cyclopentanone ring C1C2C3C4C5 is nonplanar. In conformation **b** both cyclohexane and lactone rings have chair conformations. In conformation **c** the cyclohexane and lactone rings have boat and chair conformations, respectively. To confirm that when the cyclohexane and lactone rings have chair and boat conformations, respectively, there is only one stable conformation of the cyclo-

Table 2. Conformational Analysis of Cytotoxins **1**, **2**, **3**, and **4**

molecule	conf	$\Delta E^{a,b}$	$\Delta E^{a,c}$	$\Delta G^{a,c}$	P (%)[d]
1	**a**	0.00	0.00	0.00	99.98
	b	4.93	5.43	5.09	0.02
	c	5.54	5.68	5.76	0.01
2	**a**		0.00	0.00	99.98
	b	*e*	5.01	5.01	0.02
3	**a**	0.00	0.00	0.00	99.63
	b	2.78	3.20	3.32	0.37
4	**a**	0.00	0.00	0.00	99.55
	b	5.81	2.06	3.21	0.45
	c	*e*	4.72	5.27	0.01
	d	9.74	7.83	8.85	0.00
	e	10.39	7.91	9.14	0.00
	f	15.92	11.66	13.56	0.00

[a] kcal/mol. [b] MMFF94. [c] B3LYP/6-31G*. [d] Populations calculated using ΔG values at 298 K. [e] Not found with MMFF94 either by Monte Carlo searching or by optimization starting from the B3LYP/6-31G* geometry.

Table 3. Calculated Dihedral Angles for Conformations **a** of **1**−**4** and Experimental Dihedral Angles for **1**[a,b]

	X-ray[a]		B3LYP/6-31G*			
	1		**1**	**2**	**3**	**4**
C1−C2−C3−C4	−39.7	−38.6	−33.8	−24.8	−9.7	−39.7
C2−C3−C4−C5	34.4	33.5	26.0	14.8	−13.1	38.5
C3−C4−C5−C1	−15.4	−14.9	−7.9	1.3	30.6	−23.0
C4−C5−C1−C2	−9.9	−9.9	−13.3	−16.6	−35.8	−2.0
C5−C1−C2−C3	30.9	30.6	29.8	25.7	28.7	26.2
C1−C5−C6−O	−44.7	−46.4	−42.4			
C5−C6−O−C7	51.6	57.4	52.7			
C6−O−C7−C8	−4.6	−8.9	−7.1			
O−C7−C8−C1	−45.5	−45.4	−44.4			
C7−C8−C1−C5	47.8	51.1	49.7			
C8−C1−C5−C6	−4.2	−6.3	−7.8			
C1−C2−C11−C10	74.2	74.0	75.3	74.3	74.3	74.4
C2−C11−C10−C9	−56.2	−57.9	−57.5	−58.5	−58.7	−58.3
C11−C10−C9−C8	36.1	39.7	37.6	40.1	39.9	39.6
C10−C9−C8−C1	−35.4	−38.7	−36.5	−37.6	−37.1	−36.6
C9−C8−C1−C2	56.6	58.8	57.4	57.2	56.5	56.3
C8−C1−C2−C11	−77.6	−77.4	−77.8	−77.3	−76.8	−77.1
C9−C8−C1−C5	172.9	175.5	173.7	175.9	174.7	174.6
C10−C11−C2−C3	−169.9	−169.3	−166.7	−167.1	−168.2	−168.3
C5−C4−O−C3	−178.4	−176.3	−179.5	−179.8	−179.7	

[a] X-ray crystallography: refs 2, 3. The two sets of coordinates are for the two independent molecules in the unit cell. [b] All Dihedral angles are for the 1*R* ACs of **1**-**4**.

pentanone ring, we have scanned the potential energy surface (PES), varying the dihedral angle C1C2C3C4, starting from the optimized geometry of conformation **a**, with the results shown in Figure 1. The PES exhibits only one minimum, corresponding to the C1C2C3C4 value in **a**, supporting the results of the Monte Carlo search. In addition, we have also scanned the PES with respect to the lactone ring dihedral angle C1C8C7O, starting from the optimized geometry of **a**, with the results shown in Figure 2. The PES exhibits two minima, the C1C8C7O angle for the lower energy minimum corresponding to conformation **1a**. Optimization starting from the higher energy minimum leads to conformation **1c**, showing that, in this scan, as the dihedral angle C1C8C7O reverses sign, the cyclohexane ring conformation changes from chair to boat.

In the case of **2**, only one conformation, **a**, was found via Monte Carlo searching. Key dihedral angles of the B3LYP/6-31G* structure of conformation **a** of **2** are listed in Table 3. The cyclohexane ring C1C2C11C10C9C8 has a chair conformation with dihedral angles very close to those of **1**. Since it was surprising that Monte Carlo searching did not also find a conformation of **2** containing a boat conformation of the cyclohexane ring, we built and optimized such a conformation using B3LYP/6-31G*. A stable conformation, **b**, was found with the relative energy and free energy given in Table 2. The equilibrium population of **a** is predicted to be >99% (Table 2); as with **1**, **2** is effectively conformationally

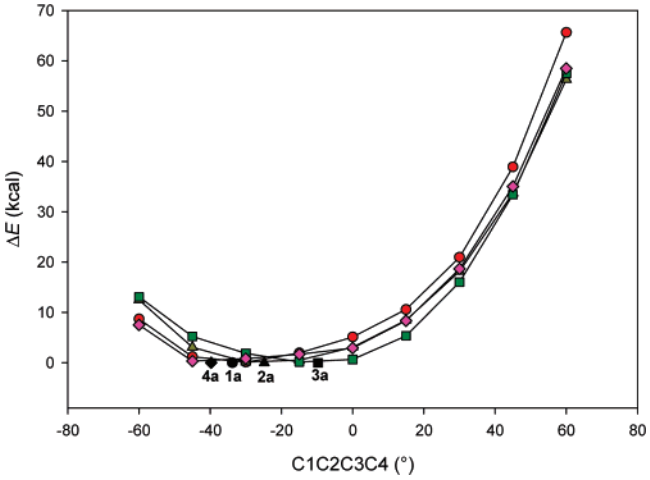

Figure 1. B3LYP/6-31G* energies of **1**−**4** as a function of the dihedral angle C1C2C3C4: **1** (red ●), **2** (olive ▲), **3** (green ■), and **4** (magenta ◆). C1C2C3C4 values for the optimized geometries of **1a** (●), **2a** (▲), **3a** (■), and **4a** (◆) are also shown.

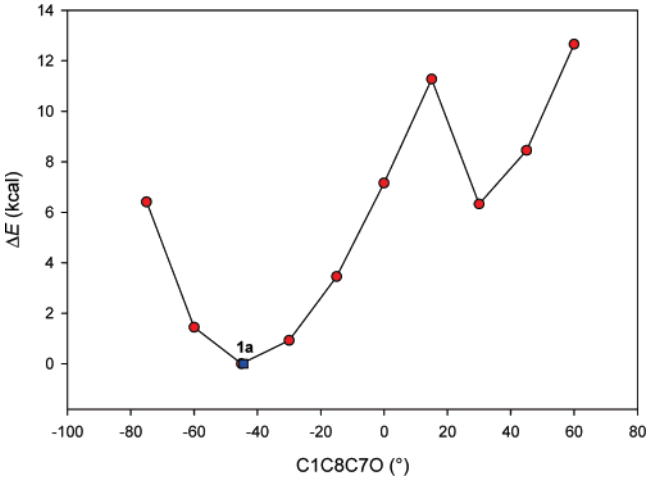

Figure 2. B3LYP/6-31G* energy of **1** as a function of the dihedral angle C1C8C7O. The C1C8C7O value for the optimized geometry of **1a** (blue ■) is also shown.

rigid. The conformation of the cyclopentanone ring C1C2C3C4C5 is similar to that of **1**. A scan, starting from the optimized geometry of conformation **a**, varying the dihedral angle C1C2C3C4, again finds no additional PES minima for the cyclopentanone ring (Figure 1), supporting the results of the Monte Carlo search.

In the case of **3**, two stable conformations, **a** and **b**, are identified. As with **1**, MMFF94 and B3LYP/6-31G* relative energies are very similar, as are B3LYP/6-31G* relative energies and free energies (Table 2). The equilibrium population at room temperature of the most stable conformation, **a**, is predicted to be >99% (Table 2); as with **1** and **2**, **3** is effectively conformationally rigid. Key dihedral angles of the B3LYP/6-31G* structure of conformation **a** of **3** are listed in Table 3. The cyclohexane ring C1C2C11C10C9C8 has a chair conformation, with dihedral angles very close to those of **1** and **2**. The conformation of the cyclopentanone ring C1C2C3C4C5, in contrast, is very different from that of **1** and of **2**. A scan, starting from the optimized geometry of conformation **a**, varying the dihedral angle C1C2C3C4, again finds no additional PES minima for the cyclopentanone ring (Figure 1), supporting the results of the Monte Carlo search. In conformation **b**, the cyclohexane ring has a boat conformation.

Molecule **4** is more conformationally flexible than **2** and **3** since internal rotation of the acetate group can occur around the C−O bond and since the acetate group can be *cis* or *trans*. MMFF94 Monte Carlo searching led to five conformations, labeled **a**, **b**, **d**,

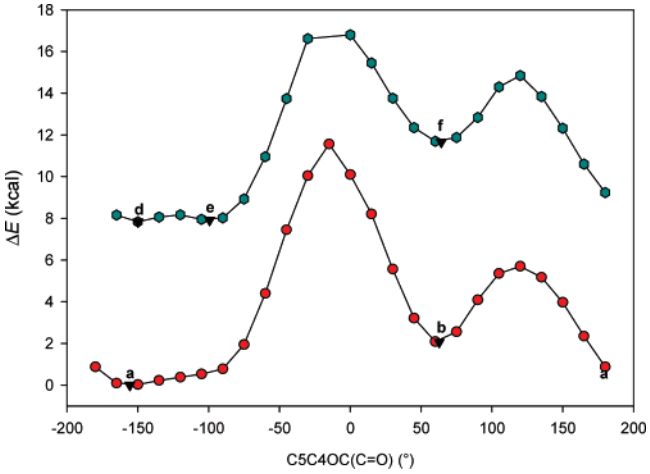

Figure 3. B3LYP/6-31G* energy of **4** as a function of the dihedral angle C5C4OC(C═O) for the *cis* (red ●) and *trans* (teal ⬢) acetate group conformations. C5C4OC(C═O) values for the optimized geometries of **4a**−**4f** (▼) are also shown.

e, and **f** in Table 2. Key dihedral angles of the B3LYP/6-31G* structure of conformation **a** of **4** are listed in Table 3. In all of these conformations the cyclohexane ring is in a chair conformation. In **a** and **b** the acetate group is *cis*; in **d**, **e**, and **f** it is *trans*. PES scans with respect to the dihedral angle C5C4OC(C═O), starting from conformations **a** and **d**, are shown in Figure 3 and support the Monte Carlo search results. As with **2**, Monte Carlo searching did not find any conformation of **4** in which the cyclohexane ring has a boat conformation. Converting the cyclohexane ring of conformation **a** from chair to boat and optimization using B3LYP/6-31G* led to the stable conformation **c**. It is likely that conformations analogous to conformations **b**, **d**, **e**, and **f** with boat cyclohexane rings exist also at energies higher than conformation **c**. On the basis of conformations **a**−**f**, the equilibrium population at room temperature of **a** is predicted to be >99% (Table 2); as with **1**−**3**, **4** is effectively conformationally rigid.

Specific Rotations, $[\alpha]_D$. Specific rotations have been calculated for conformations **a** of **1**−**4** at the sodium D line using the TDDFT/GIAO methodology at the B3LYP/aug-cc-pVDZ level and the B3LYP/6-31G* geometries, with the results given in Table 1, where the experimental specific rotations for the naturally occurring enantiomers are also listed.

In the case of **1**, calculated $[\alpha]_D$ values for the 1*R*,2*R*,5*S*,8*R*,11*R* and 1*S*,2*S*,5*R*,8*S*,11*S* enantiomers are −38.8 and +38.8, respectively. The differences, $\Delta = [\alpha]_D(\text{calc}) - [\alpha]_D(\text{expt})$, are +13.9/21.73 and +91.5/99.33, respectively, for the two literature experimental values of $[\alpha]_D$. (Note that these were measured in different solvents, EtOH and $CHCl_3$ (Table 1); the difference in $[\alpha]_D$ values may therefore be due either to a difference in enantiomeric excess or to solvent effects.) The calculated $[\alpha]_D$ is thus much closer to the experimental $[\alpha]_D$ for naturally occurring **1** for the 1*R*,2*R*,5*S*,8*R*,-11*R* AC, and we conclude that this is the AC of (−)-**1**. This AC is in agreement with the AC obtained by Smith et al.[3] In the case of **2**, calculated $[\alpha]_D$ values for the 1*R*,2*R*,8*R*,11*R* and 1*S*,2*S*,8*S*,11*S* enantiomers are 10.5 and −10.5, respectively. The differences from the experimental $[\alpha]_D$ of naturally occurring **2** are −45.2 and −66.2, respectively, leading to the more tentative conclusion that 1*R*,2*R*,8*R*,-11*R* is the AC of (+)-**2**. In the case of **3**, calculated $[\alpha]_D$ values for the 1*R*,2*R*,5*S*,8*R*,11*R* and 1*S*,2*S*,5*R*,8*S*,11*S* enantiomers are −20.6 and +20.6, respectively. The differences from the experimental $[\alpha]_D$ of naturally occurring **3**, Δ, are +39.4 and +80.6, respectively, leading to the conclusion that 1*R*,2*R*,5*S*,8*R*,11*R* is the AC of (−)-**3**. In the case of **4**, calculated $[\alpha]_D$ values for the 1*R*,2*R*,4*R*,8*R*,-11*R* and 1*S*,2*S*,4*S*,8*S*,11*S* enantiomers are −220.8 and +220.8, respectively. The differences from the experimental $[\alpha]_D$ of naturally occurring **4** are −110.8 and 330.8, respectively, leading to the conclusion that 1*R*,2*R*,4*R*,8*R*,11*R* is the AC of (−)-**4**.

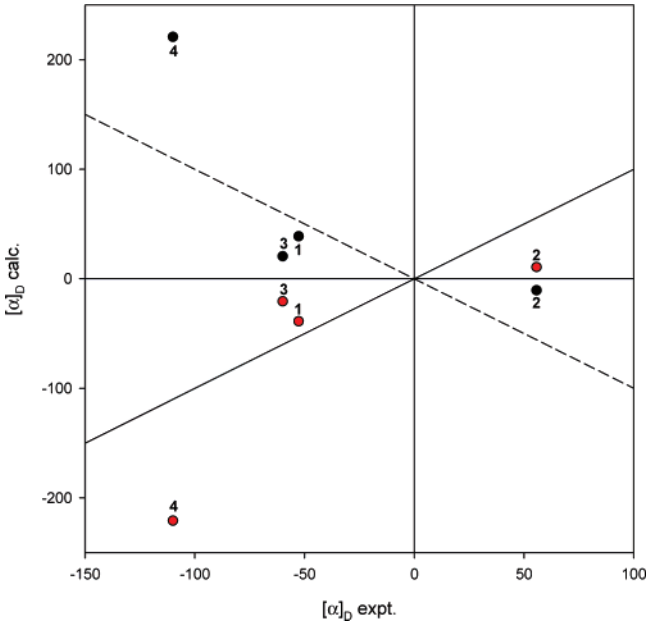

Figure 4. Comparison of calculated and experimental $[\alpha]_D$ values of **1**−**4**: (red ●) (1*R*,2*R*,5*S*,8*R*,11*R*)-**1**, (1*R*,2*R*,8*R*,11*R*)-**2**, (1*R*,2*R*,5*S*,8*R*,-11*R*)-**3**, 1*R*,2*R*,4*R*,8*R*,11*R*)-**4**; (black ●) (1*S*,2*S*,5*R*,8*S*,11*S*)-**1**, (1*S*,2*S*,8*S*,11*S*)-**2**, (1*S*,2*S*,5*R*,8*S*,11*S*)-**3**, (1*S*,2*S*,4*S*,8*S*,11*S*)-**4**. The lines have slopes of +1 and −1.

Calculated $[\alpha]_D$ values for both enantiomers of **1**−**4** are compared graphically to the experimental $[\alpha]_D$ values for the natural products in Figure 4. Quantitatively perfect calculations for correct ACs give $[\alpha]_D$ values lying on the line of slope +1. For incorrect ACs $[\alpha]_D$ values will lie on the line of slope −1.

Our $[\alpha]_D$ calculations thus lead to the conclusion that the common tricyclic core of all four natural product molecules **1**−**4** is of identical absolute configuration.

Electronic Circular Dichroism. Electronic excitation energies and rotational strengths have been calculated for conformations **a** of **1**−**4** using TDDFT at the B3LYP/aug-cc-pVDZ level and the B3LYP/6-31G* geometries, with the results given in Table 1 of the Supporting Information and Figure 5. The experimental CD spectrum of (−)-**1**[3] is also given in Figure 5. In the case of **1**, the lowest excitation, the n → π^* transition of the ketone group, is predicted at 300 nm. For the 1*R*,2*R*,5*S*,8*R*,11*R* AC, the predicted rotational strength is positive. The spectrum becomes more dense at λ < 225 nm, with nine transitions predicted between 190 and 225 nm. The rotational strengths of these transitions vary in sign and magnitude. The CD spectra of **1**, calculated using Gaussian band shapes of two different widths (σ = 0.2, 0.4 eV), are also shown in Figure 5. The agreement between calculated and experimental spectra is very good, over the relatively limited spectral range of the experimental spectrum. The positive CD at 298 nm and the negative CD at 216 nm are reproduced by the calculations. The CD calculations thus lead to the conclusion that the AC of **1** is 1*R*,2*R*,5*S*,8*R*,11*R*-(−), in agreement with the AC derived from $[\alpha]_D$ and the AC of Smith et al.[3]

In the cases of **2** and **3**, the ketone n → π^* excitations are predicted at 367 and 296 nm, respectively. For (1*R*,2*R*,8*R*,11*R*)-**2** and (1*R*,2*R*,5*S*,8*R*,11*R*)-**3**, the rotational strengths and CD of these transitions are both predicted to be positive. At shorter wavelengths, the CD spectrum becomes more dense and complex. In the case of **4**, there is no low-energy resolved excitation: the lowest excitation is at 219 nm.

Optical Rotatory Dispersion. Specific rotations have also been calculated for the four wavelengths 578, 546, 436, and 365 nm,

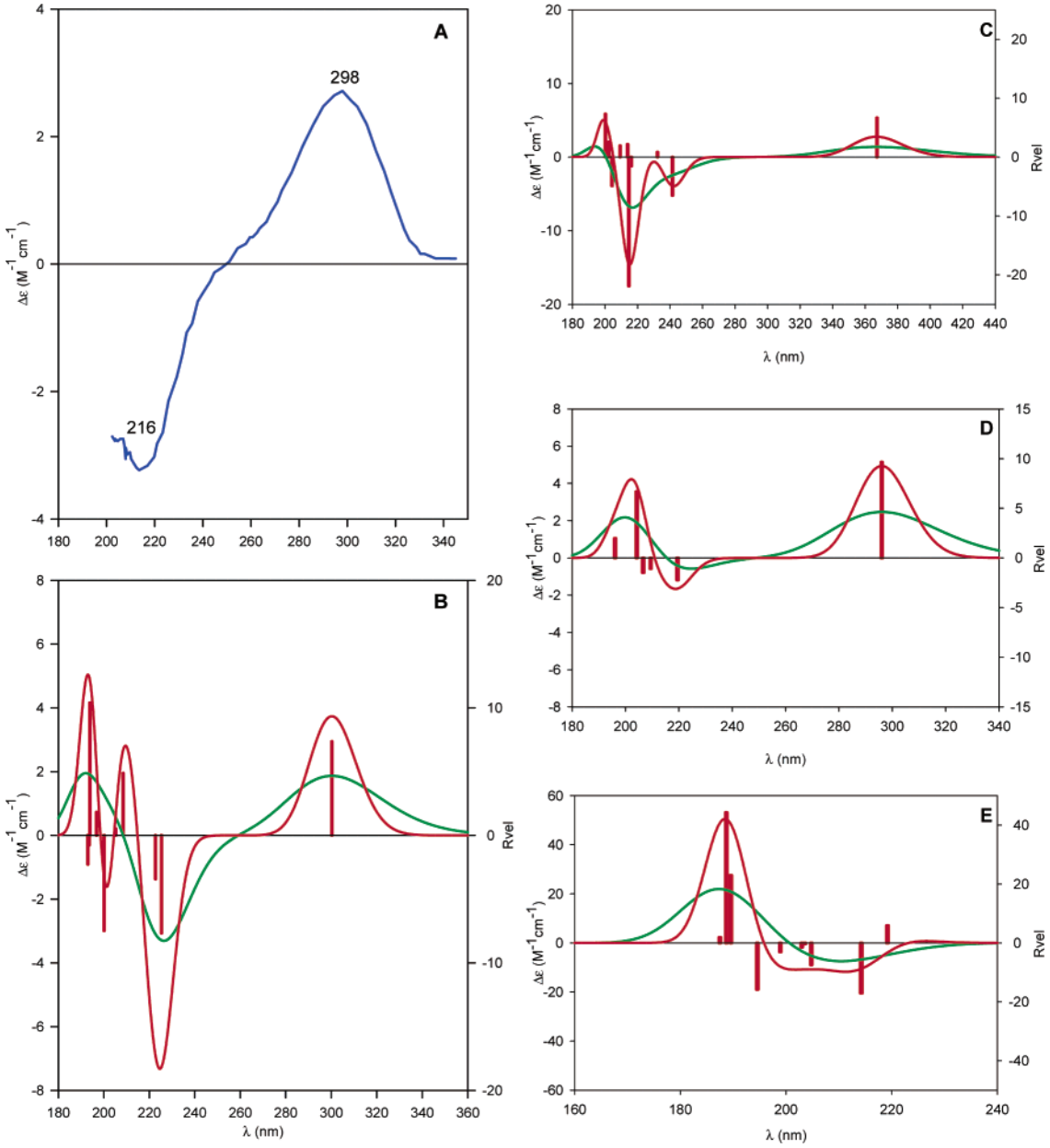

Figure 5. (A) Experimental ECD spectrum of naturally occurring (−)-**1** in MeOH, from ref 3. (B) Velocity representation B3LYP/aug-cc-pVDZ//B3LYP/6-31G* rotational strengths and simulated ECD spectrum of (1*R*,2*R*,5*S*,8*R*,11*R*)-**1** (red line, $\sigma = 0.2$ eV; green line, $\sigma = 0.4$ eV). (C) Velocity representation B3LYP/aug-cc-pVDZ//B3LYP/6-31G* rotational strengths and simulated ECD spectrum of (1*R*,2*R*,8*R*,-11*R*)-**2** (red line, $\sigma = 0.2$ eV; green line, $\sigma = 0.4$ eV). (D) Velocity representation B3LYP/aug-cc-pVDZ//B3LYP/6-31G* rotational strengths and simulated ECD spectrum of (1*R*,2*R*,5*S*,8*R*,11*R*)-**3** (red line, $\sigma = 0.2$ eV; green line, $\sigma = 0.4$ eV). (E) Velocity representation B3LYP/aug-cc-pVDZ//B3LYP/6-31G* rotational strengths and simulated ECD spectrum of (1*R*,2*R*,4*R*,8*R*,11*R*)-**4** (red line, $\sigma = 0.2$ eV, green line, $\sigma = 0.4$ eV).

routinely available in commercial polarimeters, with the results given in Table 1. In the case of **1**, [α] rises very slightly in magnitude from the sodium D line to 546 nm, then decreases at 436 nm and crosses zero to become large and positive at 365 nm. This behavior can be explained as follows. The specific rotation at wavelength λ, $[\alpha]_\lambda$, is given by

$$[\alpha]_\lambda = \sum_i [\alpha]_\lambda^i$$

$$[\alpha]_\lambda^i = \left(\frac{9147}{M}\right)\frac{R_i {\lambda_i}^2}{{\lambda_i}^2 - \lambda^2}$$

where λ_i and R_i are the wavelength and rotational strength of excitation i. At the sodium D line, for (1*R*,2*R*,5*S*,8*R*,11*R*)-**1** [α] is predicted to be negative. As λ decreases, $1/({\lambda_i}^2 - \lambda^2)$ increases and [α] becomes increasingly negative. However, as λ approaches the lowest excitation wavelength (300 nm), the contribution of this excitation to [α] increases more rapidly than that of higher energy excitations. Since the rotational strength of the lowest excitation is positive, as 300 nm is approached, [α] crosses zero and becomes positive.

In the case of **2**, $[\alpha]_D$ is the same sign as the rotational strength of the lowest excitation, now at 367 nm, and [α] increases monotonically with decreasing wavelength to 436 nm. In the case of **3**, [α] decreases in magnitude from the sodium D line to 546 nm, then crosses zero to become positive at 436 and 365 nm. This behavior is qualitatively identical to that of **1**, and the explanation is the same. In the case of **4**, as in **1** and **3**, $[\alpha]_D$ is opposite in sign to the rotational strength of the lowest excitation. Unlike **1** and **3**,

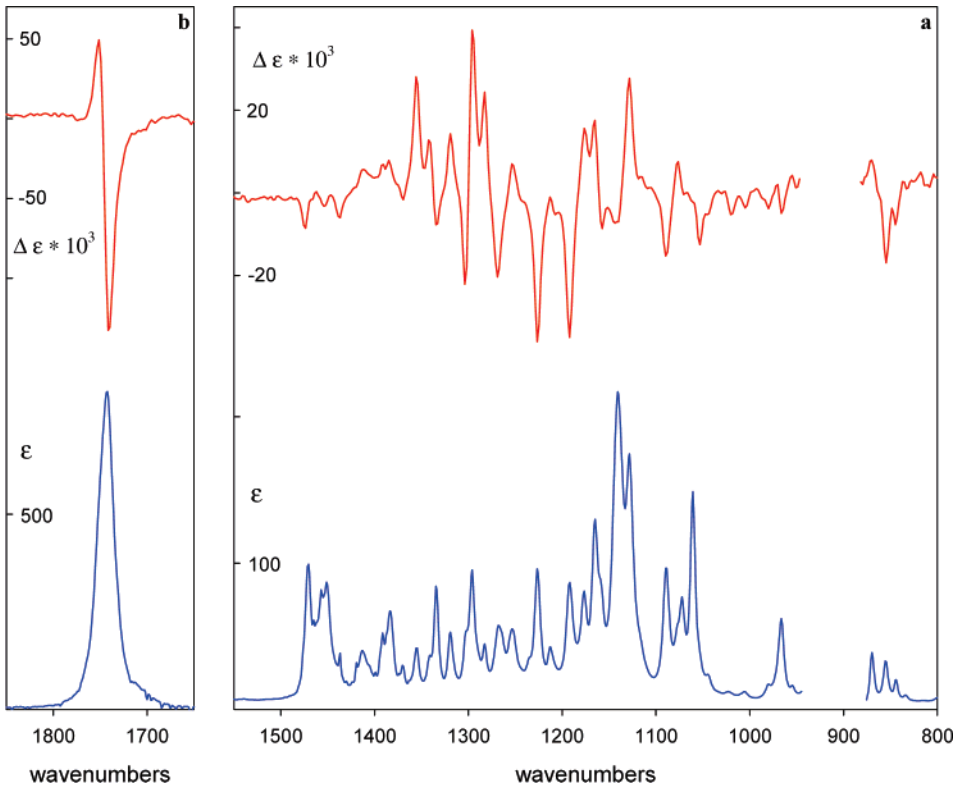

Figure 6. Experimental IR and VCD spectra of (−)-**1**: 0.24 M (a) and 0.14 M (b) in $CDCl_3$.

however, [α] increases monotonically from the sodium D line to 365 nm, due to the much higher energy of the lowest excitation (λ = 219 nm).

For **1** we have measured the specific rotation of (−)-**1**, synthesized as described previously,[3] in $CDCl_3$ at the sodium D line and at the wavelengths 578, 546, 436, and 365 nm. The qualitative variation of $[\alpha]_\lambda$ with λ is exactly as predicted, supporting the reliability of the TDDFT/GIAO methodology. Quantitatively, the differences between calculated and experimental $[\alpha]_\lambda$ values vary little with λ, except at 365 nm.

Vibrational Circular Dichroism. The IR and VCD spectra of (−)-**1**, synthesized as described previously,[3] in $CDCl_3$ solution in the mid-IR spectral region are shown in Figure 6. DFT calculations of the IR and VCD spectra of conformation **a** of (1*R*,2*R*,5*S*,8*R*,11*R*)-**1** have been carried out, using the B3LYP and B3PW91 functionals, which are both state-of-the-art hybrid functionals, and the TZ2P basis set, which we have shown to provide a good compromise between computational labor and accuracy in predicting VCD spectra.[12h] Calculated harmonic vibrational frequencies, dipole strengths, and rotational strengths are given in Table 2 of the Supporting Information (SI). IR and VCD spectra obtained thence using Lorentzian band shapes are also given in Figures 1 and 2 of the SI, together with the experimental spectra. Comparison of the calculated IR and VCD spectra to the corresponding experimental spectra of (−)-**1** shows that the B3PW91 IR and VCD spectra are in better agreement with experiment than the B3LYP spectra. The B3PW91-calculated IR and VCD spectra, together with the experimental spectra, are shown in Figures 7 and 8. Assignment of the experimental spectra follows straightforwardly, as shown in Figures 7 and 8. The excellent agreement of the calculated VCD spectrum for (1*R*,2*R*,5*S*,8*R*,11*R*)-**1** and the experimental VCD spectrum for (−)-**1** leads to the conclusion that the AC of **1** is (1*R*,2*R*,5*S*,8*R*,11*R*)-(−). The AC is further confirmed by comparison of the calculated rotational strengths and the experimental rotational strengths, obtained by Lorentzian fitting of the experimental VCD spectrum. The experimental rotational strengths, together with the experimental frequencies, dipole strengths, and bandwidths, are given in Table 2 of the SI. They are compared to the calculated rotational strengths for the two possible ACs in Figure 9. Clearly, the agreement is enormously superior for the 1*R*,2*R*,5*S*,8*R*,11*R* AC.

In predicting the specific rotations, ECD, and VCD of a chiral molecule, it is necessary first to establish how many conformations are populated at room temperature (the temperature of the experimental measurements). When more than one conformation is significantly populated, the chiroptical properties of each conformation must be predicted and population-weighted averages calculated. In the case of all four molecules, **1**−**4**, conformational analyses lead to the conclusion that only one conformation, **a**, is populated at room temperature. From a practical point of view, therefore, all four molecules are conformationally rigid. In the case of **1**, this conclusion is consistent with the temperature-independence of the NMR spectrum.[3] The reliability of the predicted structure of **1a** is confirmed by comparison to the structure determined by X-ray crystallography.[1b,3] As shown in Table 1, the dihedral angles of the cyclohexane, cyclopentanone, and lactone rings of **1a** predicted at the B3LYP/6-31G* level are in excellent agreement with the experimental values for the two independent molecules in crystalline **1**. The largest differences are found for the cyclopentanone ring, but they are all <10°. In all four molecules, the cyclohexane ring of conformation **a** exhibits a chair conformation, whose predicted dihedral angles vary very little (Table 3). In contrast, the conformation of the five-membered C1C2C3C4C5 ring varies considerably with the varying substitution.

Assignment of the absolute configurations of **1**−**4** using their $[\alpha]_D$ values then proceeds as follows. For both possible enantiomers of each molecule $[\alpha]_D$ is predicted and compared to the experimental value. The enantiomer for which the difference between calculated and experimental $[\alpha]_D$ values is smallest is the AC corresponding to the experimental rotation. The $[\alpha]_D$ calculations are carried out using the B3LYP functional and the aug-cc-pVDZ basis set. The former is a state-of-the-art hybrid functional. The latter contains diffuse functions, which have been shown to be required for reliable $[\alpha]_D$ predictions,[7b] and provides a good approximation to the complete basis set limit.[7b,c] In the cases of **1**, **3**, and **4**, the differences, $\Delta = [\alpha]_D(\text{calc}) - [\alpha]_D(\text{expt})$, are much smaller for one enantiomer, as compared to the opposite enantiomer. As a

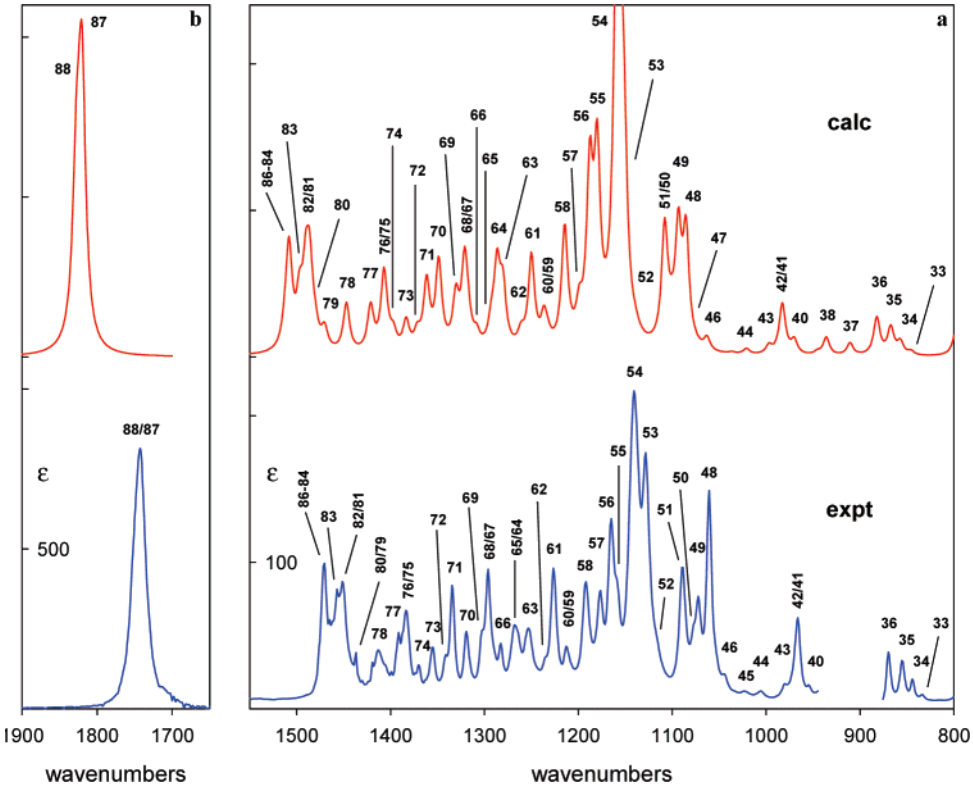

Figure 7. Calculated, B3PW91/TZ2P, and experimental IR spectra of (−)-**1** in the mid-IR spectral region. Fundamentals are numbered. Lorentzian bandwidths are 4 cm^{-1} (a) and 6 cm^{-1} (b).

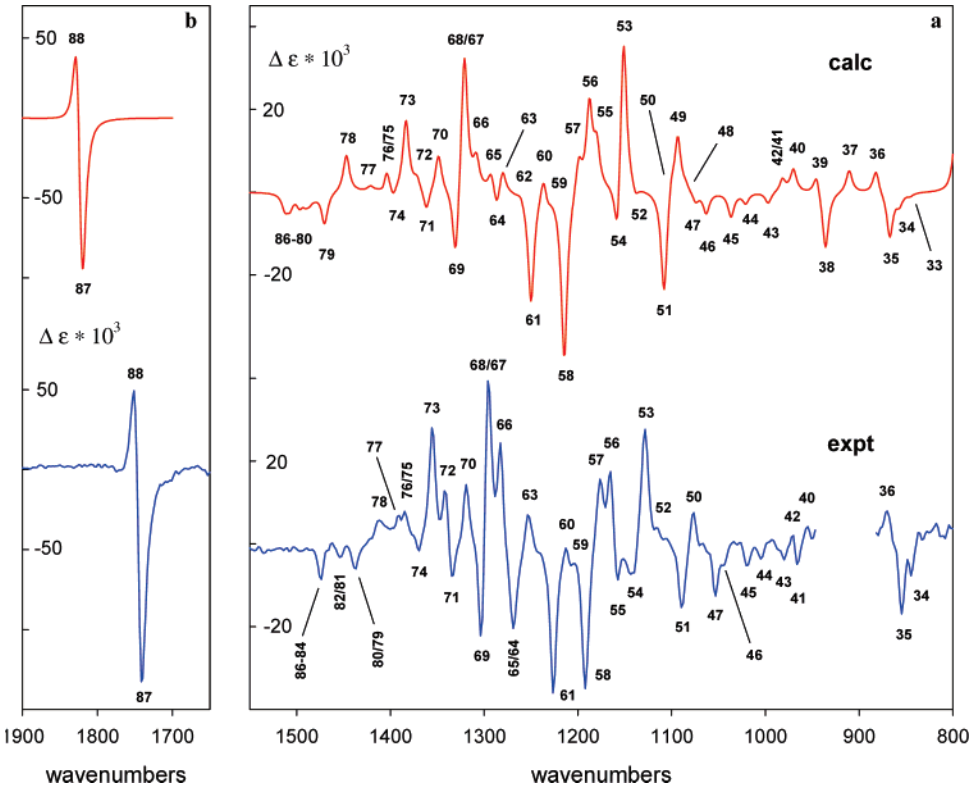

Figure 8. Calculated, B3PW91/TZ2P VCD spectrum of (1*R*,2*R*,5*S*,8*R*,11*R*)-**1** and experimental VCD spectrum of (−)-**1** in the mid-IR spectral region. Fundamentals are numbered. Lorentzian bandwidths are 4 cm^{-1} (a) and 6 cm^{-1} (b).

result, there is little uncertainty in the assigned ACs: (1*R*,2*R*,5*S*,8*R*,-11*R*)-(−) for **1**, (1*R*,2*R*,5*S*,8*R*,11*R*)-(−) for **3**, and (1*R*,2*R*,4*R*,8*R*,-11*R*)-(−) for **4**. In the case of **2**, the calculated $[\alpha]_D$ is small in magnitude (10.5) and the differences Δ are not very different (−45.2 and −66.2). Accordingly, there is greater uncertainty in the AC assignment for **2**, (1*R*,2*R*,8*R*,11*R*)-(+).

The AC of **1** has been previously established via total synthesis of (+)- and (−)-**1** by Smith et al.[3] The AC determined from our $[\alpha]_D$ calculation is the same as that of Smith et al., providing support for the TDDFT/GIAO methodology, implemented at the B3LYP/aug-cc-pVDZ//B3LYP/6-31G* level.

In the cases of **2**−**4**, ACs have not previously been assigned. It

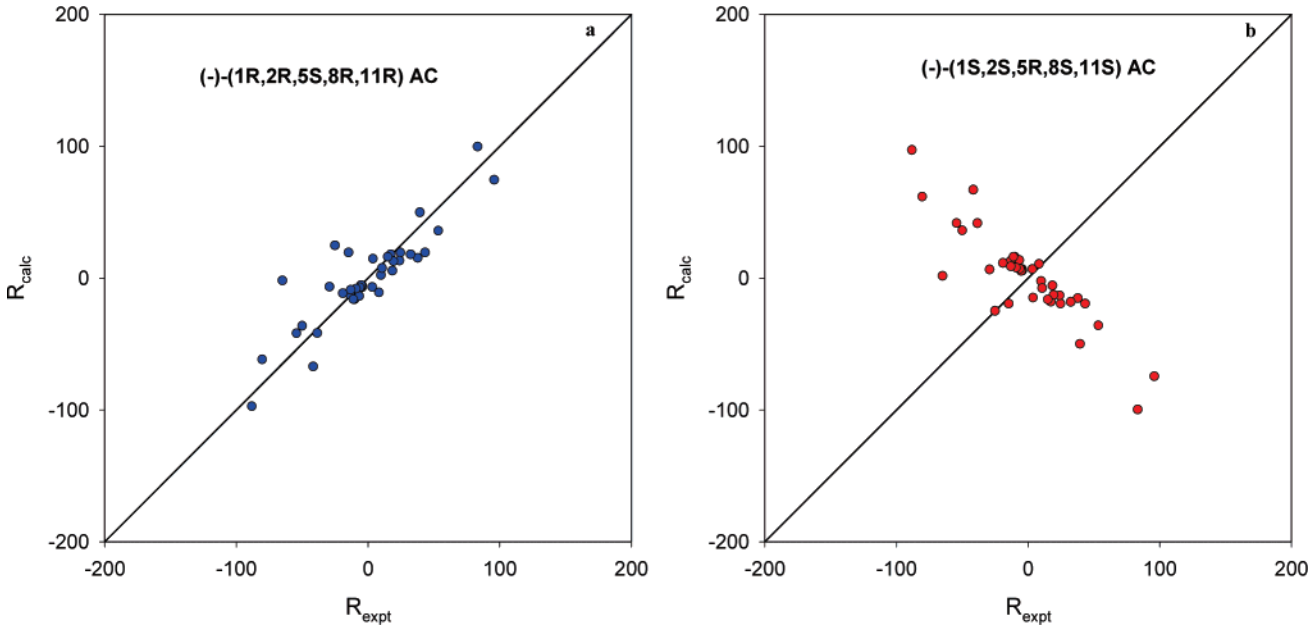

Figure 9. Comparison of experimental rotational strengths for (−)-**1** with the B3PW91/TZ2P rotational strengths for (1*R*,2*R*,5*S*,8*R*,11*R*)-**1** (a) and (1*S*,2*S*,5*R*,8*S*,11*S*)-**1** (b). The lines have slopes of +1.

follows from the ACs we have assigned that the naturally occurring forms of all four molecules possess identical absolute configurations of their common tricyclic cores. The fact that the configurations of **3** and **4** are found to be identical provides further support for the ACs assigned since these two natural products were obtained from the same organism, *I. hippuris*, and therefore most likely possess identical configurations. That the absolute configurations of **1**, **2**, **3**, and **4** are all identical leads to the conclusion that the biosynthetic pathways leading to these molecules in *A. terreus*, *S. suberosa*, and *I. hippuris* proceed with the same absolute stereogenicity.

Calculated $[\alpha]_D$ values are not in perfect agreement with experimental values. The errors in calculated $[\alpha]_D$ values could be due to errors in the functional, B3LYP, the basis set, aug-cc-pVDZ, and/or the geometry, B3LYP/6-31G*. Alternatively, they could originate in vibrational effects and solvent effects, which are neglected in our calculations. We have recently carried out an extensive evaluation of the reliability of B3LYP/aug-cc-pVDZ//B3LYP/6-31G* $[\alpha]_D$ calculations for 65 conformationally rigid molecules of known AC whose experimental $[\alpha]_D$ values are <100.[16] The results are shown graphically in Figure 10. The rms deviation, σ, of calculated and experimental $[\alpha]_D$ values for this set of molecules is 28.9. Thus, statistically, with 95% confidence, calculated $[\alpha]_D$ values should differ from experimental values by less than $2\sigma = 57.8$. As shown in Figure 10, for the correct AC all molecules lie between the parallel lines of slope +1 and intercepts +57.8 and −57.8 (with three exceptions, which are just outside these limits). For the incorrect AC, all molecules lie between the parallel lines of slope −1 and intercepts +57.8 and −57.8. The region where molecules lie between *both* pairs of parallel lines is labeled "the zone of indeterminacy".[16] The AC of a molecule within this zone cannot be determined with 95% confidence from its $[\alpha]_D$ value.

The calculated and experimental $[\alpha]_D$ values of molecules **1**, **2**, **3**, and **4** are also shown in Figure 10 for the ACs arrived at above. Molecules **1**−**3** lie outside the zone of indeterminacy (although only by a very small margin in the case of **2**) and between the lines of slope +1. Molecule **4** is not close to the zone of indeterminacy, but it lies outside the lines of slope +1. It follows that the errors in calculated $[\alpha]_D$ values for **1**−**3** are statistically typical of B3LYP/aug-cc-pVDZ//B3LYP/6-31G* calculations, neglecting vibrational and solvent effects, and that the ACs can be assigned with 95% confidence. For **4**, the error is larger than statistically typical, somewhat reducing the confidence level of the AC arrived at. However, for molecules with $[\alpha]_D$ values > 100 we have not yet encountered any cases where the sign is incorrectly predicted. It is therefore very unlikely that the assigned AC of **4** is incorrect.

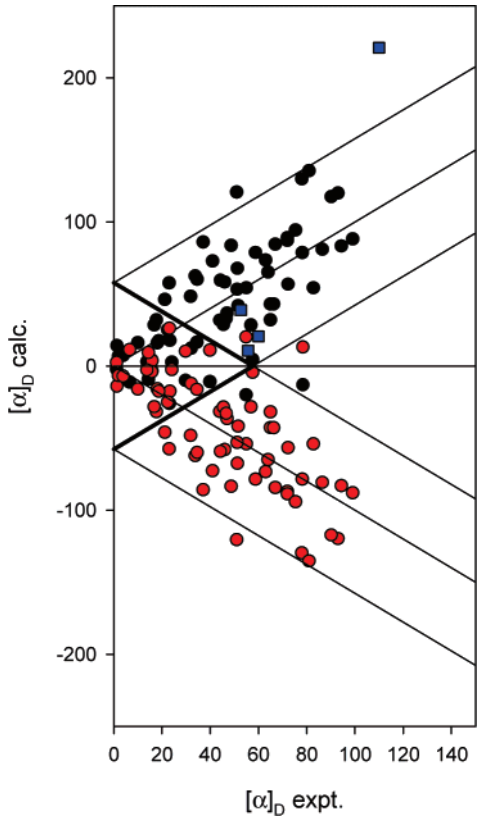

Figure 10. Comparison of experimental and calculated $[\alpha]_D$ for 65 molecules. Enantiomers are chosen with positive experimental $[\alpha]_D$ values. (black ●) Correct ACs; (red ●) opposite ACs. The *y*-axis intercepts of the straight lines are 0, $+2\sigma$, and -2σ, where $2\sigma = 57.8$. The triangular area bounded by the boldfaced lines is "the zone of indeterminacy". (blue ■) Cytotoxins **1**−**4**.

The ECD spectrum of (−)-**1** was reported by Smith et al.,[3] but to date ECD spectra for **2**−**4** have not been reported. In order to

further confirm the AC of **1**, and in order to define the potential utility of ECD in further confirming the ACs of **2**−**4**, we have carried out TDDFT calculations of the ECD of **1**−**4**. As expected, **1**, **2**, and **3** exhibit one low-energy excitation attributable to n → π^* excitations of their carbonyl groups. In **1** and **3**, these excitations are near 300 nm; in **2** conjugation red shifts this excitation to ~370 nm. For (1*R*,2*R*,5*S*,8*R*,11*R*)-**1** the rotational strength is positive, the sign of the experimental ECD of (−)-**1**, consistent with the AC of Smith et al. For (1*R*,2*R*,8*R*,11*R*)-**2** and (1*R*,2*R*,5*S*,8*R*,11*R*)-**3**, the predicted rotational strengths are also positive and similar in magnitude to **1**. The excitations at higher energies are much more closely spaced and the ECD spectra predicted are sensitive to the bandwidths of these excitations. In the case of **1**, the negative ECD observed experimentally at 216 nm is successfully predicted, but it is uncertain how well the experimental spectrum below this wavelength is reproduced. In the case of **4**, there is no well-resolved, lower energy excitation, and the predicted spectrum is dense and complex. We conclude that ECD studies of the n → π^* carbonyl excitations of **2** and **3** will be useful in further confirming their ACs, but that studies of the shorter wavelength ECD of **2**−**4** are less likely to be useful for this purpose.

VCD spectroscopy provides an alternative chiroptical technique for determining the ACs of chiral molecules. The availability of a synthetic sample of nearly optically pure (−)-**1** has enabled the measurement of the VCD spectrum of **1** for the first time, the further confirmation of the AC of **1**, and the demonstration of the power of the VCD technique, relative to the optical rotation and ECD techniques, in determining ACs. The VCD spectrum of (−)-**1** over the frequency range 800−1800 cm^{-1}, shown in Figure 6, exhibits many well-resolved bands with high signal-to-noise ratios. Analysis of this spectrum follows the protocol that we (at USC) have developed and applied to a wide range of chiral molecules. The first step is the assignment of the IR spectrum, based on DFT calculations using the TZ2P basis set and the functionals B3LYP and B3PW91. The TZ2P basis set has been shown to provide a good approximation to the complete basis set limit and to be far more accurate in predicting IR and VCD spectra than small basis sets such as 6-31G*.[12h] The B3LYP and B3PW91 hybrid functionals are state-of-the-art, but not identical. Use of both functionals permits the sensitivity of the calculated spectra to the choice of functional to be gauged and the more reliable functional for the specific molecule under study to be selected. The B3LYP/TZ2P and B3PW91/TZ2P IR spectra of **1**, shown in Figure 1 of the SI, are very similar overall, but not identical: see, for example, the very different relative intensities of fundamentals 53 and 54. Comparison with the experimental spectrum permits unambiguous assignment of the large majority of the observed bands. For modes 53 and 54, the B3PW91/TZ2P spectrum is in better agreement with experiment. The overall excellence of the agreement of the B3PW91/TZ2P and experimental IR spectra is shown in Figure 7. The assignment of the IR spectrum simultaneously assigns the experimental VCD spectrum. The determination of the AC of **1** then simply requires the comparison of the calculated VCD spectra for the two possible ACs to the experimental spectrum. As shown in Figure 8 and Figure 2 of the SI, the calculated B3PW91/TZ2P VCD spectrum for (1*R*,2*R*,5*S*,8*R*,11*R*)-**1** is in magnificent agreement with the experimental spectrum of (−)-**1**. For every observed band, calculated and experimental VCD agree in sign. In contrast, for the opposite AC, calculated and experimental VCD signs are uniformly opposite. It follows immediately that the AC of **1** must be (1*R*,2*R*,5*S*,8*R*,11*R*)-(−). Quantitative verification of this conclusion is provided by the comparison of calculated and experimental rotational strengths. The latter are obtained by Lorentzian fitting, in which initial choices of frequencies and bandwidths are obtained from prior fitting of the IR spectrum (which always has a higher signal-to-noise ratio than the VCD spectrum). As shown in Figure 9, calculated B3PW91/TZ2P rotational strengths for the (1*R*,2*R*,5*S*,8*R*,11*R*) AC exhibit excellent quantitative agreement with experimental values. The differences between calculated and experimental rotational strengths can be attributed to a variety of factors: imperfection of the B3PW91 functional, basis set error, neglect of anharmonicity and solvent effects, and errors in experimental rotational strengths due to instrumental artifacts. In the case of calculated rotational strengths for the opposite AC the correlation with experimental values is negligible. Thus to an extremely high degree of certainty, the AC of **1** is (1*R*,2*R*,5*S*,8*R*,11*R*)-(−).

The application of the VCD technique to the determination of the AC of **1** permits the use of the VCD and ECD techniques for this purpose to be compared. The most dramatic difference is in the number and resolution of transitions. In the VCD spectrum of **1** over the range 800−1800 cm^{-1} there are 56 fundamental vibrational transitions, a large fraction of which are resolved due to the narrow bandwidths of fundamental vibrational transitions in liquid solutions. In the ECD spectrum of **1** at wavelengths > 200 nm only two bands are observed. At wavelengths < 200 nm more bands undoubtedly exist, but, as can be seen in Figure 5, given the large bandwidths of electronic excitations, few bands, if any, are likely to be resolved. Accordingly, the information content of a VCD spectrum is enormously greater than that of an ECD spectrum. From the theoretical standpoint, VCD also has the advantage that calculations involve only the ground electronic state, whereas ECD calculations involve excited electronic states. Since, with any ab initio methodology, ground electronic states are more reliably described than excited states, the frequencies and rotational strengths of vibrational transitions are more reliably predicted than for electronic transitions. Our results for **1** provide one more example of the exceptionally high reliability of DFT calculations of VCD spectra, given optimum choices of functional and basis set. It follows that VCD spectroscopy is substantially more reliable than ECD spectroscopy in determining ACs of chiral molecules. As a result, we recommend that further confirmation of the ACs of molecules **2**−**4** be carried out using the VCD technique.

Conclusion

We have demonstrated the application of DFT calculations of the optical rotation, ECD, and VCD to the determination of the ACs of chiral natural products. In the case of quadrone, **1**, the same AC, (1*R*,2*R*,5*S*,8*R*,11*R*)-(−), is obtained from all three chiroptical properties, demonstrating the reliability of the DFT methodologies. The simultaneous application of all three chiroptical spectroscopies to the same molecule also permits the relative reliabilities of the ACs obtained to be assessed, with the clear conclusion that the VCD technique leads to ACs of the highest reliability. In the cases of suberosenone, **2**, suberosanone, **3**, and suberosenol A acetate, **4**, the only chiroptical data currently available are $[\alpha]_D$ values, and our determination of their ACs is based on these properties alone. Clearly, ECD and, especially, VCD studies of these molecules are very desirable in order to definitively confirm the results obtained from the $[\alpha]_D$ values.

Acknowledgment. We are grateful for financial support from the National Science Foundation (to P.J.S., CHE-0209957) and the National Institutes of Health, National Cancer Institute (to A.B.S., CA-19033). We also thank the USC High Performance Computing and Communication (HPCC) facility for computer time and Dr. J. R. Cheeseman of Gaussian Inc. for his continual assistance and advice.

Supporting Information Available: Calculated electronic excitation energies, oscillator strengths, and rotational strengths of **1**−**4**; calculated and experimental vibrational frequencies, dipole strengths, and rotational strengths of **1**; calculated and experimental IR and VCD spectra of **1**. This material is available free of charge via the Internet at http://pubs.acs.org.

References and Notes

(1) Calton, G. J.; Ranieri, R. L.; Espenshade, M. A. *J. Antibiot.* **1978**, *31*, 38−42.

(2) Ranieri, R. L.; Calton, G. J. *Tetrahedron Lett.* **1978**, 499−502.
(3) Smith, A. B.; Konopelski, J. P.; Wexler, B. A.; Sprengeler, P. A. *J. Am. Chem. Soc.* **1991**, *113*, 3533−3542. For a preliminary report of this work, see: Smith, A. B.; Konopelski, J. P. *J. Org. Chem.* **1984**, *49*, 4094−4095. See also references cited in these papers.
(4) Bokesch, H. R.; McKee, T. C.; Cardellina, J. H.; Boyd, M. R. *Tetrahedron Lett.* **1996**, *37*, 3259−3262.
(5) Lee, H. Y.; Kim, B. G. *Org. Lett.* **2000**, *2*, 1951−1953.
(6) Sheu, J. H.; Hung, K. C.; Wang, G. H.; Duh, C. Y. *J. Nat. Prod.* **2000**, *63*, 1603−1607.
(7) (a) Stephens, P. J.; Devlin, F. J.; Cheeseman, J. R.; Frisch, M. J.; Mennucci, B.; Tomasi, J. *Tetrahedron: Asymmetry* **2000**, *11*, 2443−2448. (b) Cheeseman, J. R.; Frisch, M. J.; Devlin, F. J.; Stephens, P. J. *J. Phys. Chem.* **2000**, *104*, 1039−1046. (c) Stephens, P. J.; Devlin, F. J.; Cheeseman, J. R.; Frisch, M. J. *J. Phys. Chem. A* **2001**, *105*, 5356−5371. (d) Mennucci, B.; Tomasi, J.; Cammi, R.; Cheeseman, J. R.; Frisch, M. J.; Devlin, F. J.; Gabriel, S.; Stephens, P. J. *J. Phys. Chem. A* **2002**, *106*, 6102−6113.
(8) (a) Stephens, P. J.; Devlin, F. J.; Cheeseman, J. R.; Frisch, M. J.; Rosini, C. *Org. Lett.* **2002**, *4*, 4595−4598. (b) Stephens, P. J.; Devlin, F. J.; Cheeseman, J. R.; Frisch, M. J.; Bortolini, O.; Besse, P. *Chirality* **2003**, *15*, 557−564. (c) Stephens, P. J.; McCann, D. M.; Butkus, E.; Stoncius, S.; Cheeseman, J. R.; Frisch, M. J. *J. Org. Chem.* **2004**, *69*, 1948−1958. (d) Stephens, P. J.; McCann, D. M.; Devlin, F. J.; Cheeseman, J. R.; Frisch, M. J. *J. Am. Chem. Soc.* **2004**, *126*, 7514−7521. (e) McCann, D. M.; Stephens, P. J.; Cheeseman, J. R. *J. Org. Chem.* **2004**, *69*, 8709−8717.
(9) Wijeratne, E. M. K.; Turbyville, T. J.; Zhang, Z.; Bigelow, D.; Pierson, L. S.; Van Etten, H. D.; Whitesell, L.; Canfield, L. M.; Gunatilaka, A. A. L. *J. Nat. Prod.* **2003**, *66*, 1567−1573.
(10) (a) Stephens, P. J.; Devlin, F. J.; Chabalowski, C. F.; Frisch, M. J. *J. Phys. Chem.* **1994**, *98*, 11623−11627. (b) Stephens, P. J.; Devlin, F. J.; Ashvar, C. S.; Chabalowski, C. F.; Frisch, M. J. *Faraday Discuss.* **1994**, *99*, 103−119. (c) Devlin, F. J.; Finley, J. W.; Stephens, P. J.; Frisch, M. J. *J. Phys. Chem.* **1995**, *99*, 16883−16902. (d) Cheeseman, J. R.; Frisch, M. J.; Devlin, F. J.; Stephens, P. J. *Chem. Phys. Lett.* **1996**, *252*, 211−220. (e) Stephens, P. J.; Ashvar, C. S.; Devlin, F. J.; Cheeseman, J. R.; Frisch, M. J. *Mol. Phys.* **1996**, *89*, 579−594. (f) Devlin, F. J.; Stephens, P. J.; Cheeseman, J. R.; Frisch, M. J. *J. Phys. Chem.* **1997**, *101*, 6322−6333. (g) Devlin, F. J.; Stephens, P. J.; Cheeseman, J. R.; Frisch, M. J. *J. Phys. Chem.* **1997**, *101*, 9912−9924.
(11) (a) Stephens, P. J. *J. Phys. Chem.* **1985**, *89*, 748−752. (b) Stephens, P. J.; Lowe, M. A. *Annu. Rev. Phys. Chem.* **1985**, *36*, 213−241. (c) Stephens, P. J. *J. Phys. Chem.* **1987**, *91*, 1712−1715. (d) Stephens, P. J. The Theory of Vibrational Circular Dichroism. In *Encyclopedia of Spectroscopy and Spectrometry*; Academic Press: London, 2000; pp 2415−2421.
(12) (a) Ashvar, C. S.; Stephens, P. J.; Eggimann, T.; Wieser, H. *Tetrahedron: Asymmetry* **1998**, *9*, 1107−1110. (b) Aamouche, A.; Devlin, F. J.; Stephens, P. J. *Chem. Commun.* **1999**, *4*, 361−362. (c) Stephens, P. J.; Devlin, F. J. *Chirality* **2000**, *12*, 172−179. (d) Aamouche, A.; Devlin, F. J.; Stephens, P. J. *J. Am. Chem. Soc.* **2000**, *122*, 2346−2354. (e) Aamouche, A.; Devlin, F. J.; Stephens, P. J.; Drabowicz, J.; Bujnicki, B.; Mikolajczyk, M. *Chem.--Eur. J.* **2000**, *6*, 4479−4486. (f) Stephens, P. J.; Aamouche, A.; Devlin, F. J.; Superchi, S.; Donnoli, M. I.; Rosini, C. *J. Org. Chem.* **2001**, *66*, 3671−3677. (g) Devlin, F. J.; Stephens, P. J.; Scafato, P.; Superchi, S.; Rosini, C. *Tetrahedron: Asymmetry* **2001**, *12*, 1551−1558. (h) Stephens, P. J.; Devlin, F. J.; Aamouche, A. *Chirality: Physical Chemistry*; Hicks, J. M., Ed.; ACS Symposium Series 810; 2002; Chapter 2, pp 18−33. (i) Devlin, F. J.; Stephens, P. J.; Scafato, P.; Superchi, S.; Rosini, C. *Chirality* **2002**, *14*, 400−406. (j) Devlin, F. J.; Stephens, P. J.; Oesterle, C.; Wiberg, K. B.; Cheeseman, J. R.; Frisch, M. J. *J. Org. Chem.* **2002**, *67*, 8090−8096. (k) Stephens, P. J. Vibrational Circular Dichroism Spectroscopy: A New Tool for the Stereochemical Characterization of Chiral Molecules. In *Computational Medicinal Chemistry for Drug Discovery*; Bultinck, P., de Winter, H., Langenaecker W., Tollenaere, J., Eds.; Dekker: New York, 2003; Chapter 26, pp 699−725. (l) Cerè, V.; Peri, F.; Pollicino, S.; Ricci, A.; Devlin, F. J.; Stephens, P. J.; Gasparrini, F.; Rompietti, R.; Villani, C. *J. Org. Chem.* **2005**, *70*, 664−669. (m) Stephens, P. J.; McCann, D. M.; Devlin, F. J.; Flood, T. C.; Butkus, E.; Stoncius, S.; Cheeseman, J. R. *J. Org. Chem.* **2005**, *70*, 3903−3913. (n) Devlin, F. J.; Stephens, P. J.; Besse, P. *Tetrahedron: Asymmetry* **2005**, *16*, 1557−1566. (o) Devlin, F. J.; Stephens, P. J.; Bortolini, O. *Tetrahedron: Asymmetry* **2005**, *16*, 2653−2663.
(13) *SPARTAN 02*; Wavefunction Inc.: Irvine, CA, 2002, www.wavefunction.com.
(14) *GAUSSIAN 03*; Gaussian Inc.: Wallingford, CT, 2003, www.Gaussian.com.
(15) (a) Cheng, J. C.; Nafie, L. A.; Stephens, P. J. *J. Opt. Soc. Am.* **1975**, *65*, 1031−1035. (b) Nafie, L. A.; Dukor, R. K. In *Chirality: Physical Chemistry*; Hicks, J. M., Ed.; ACS Symposium Series 810; 2000; pp 79−88.
(16) Stephens, P. J.; McCann, D. M.; Cheeseman, J. R.; Frisch, M. J. *Chirality* **2005**, *17*, S52−S64.

NP060112P